Epitaxial GaN films by hyperthermal ion-beam nitridation of Ga droplets

J.W. Gerlach[*)], T. Ivanov, L. Neumann, Th. Höche[**)], D. Hirsch, B. Rauschenbach

Leibniz-Institut für Oberflächenmodifizierung (IOM), D-04318 Leipzig, Germany

Abstract

Epitaxial GaN film formation on bare 6H-SiC(0001) substrates via the process of transformation of Ga droplets to a thin GaN film by applying hyperthermal nitrogen ions is investigated. Pre-deposited Ga atoms in well-defined amounts form large droplets on the substrate surface which are subsequently nitridated at a substrate temperature of 630 °C by a low-energy nitrogen ion beam from a constricted glow-discharge ion source. The ion-beam nitridation process is monitored *in situ* by reflection high-energy electron diffraction. *Ex situ* characterization by x-ray diffraction and reflectivity techniques, Rutherford backscattering spectrometry and electron microscopy shows that the resulting GaN films have different thicknesses according to the various amounts of deposited Ga. The films are epitaxial to the substrate, exhibit a mosaic-like, smooth surface topography and consist of coalesced large domains of low defect density. Different possible transport mechanisms of reactive nitrogen species during the nitridation process are discussed and the formation of GaN films by an ion-beam assisted process is explained.

[*)] corresponding author:
Dr. Jürgen W. Gerlach,
Leibniz-Institut für Oberflächenmodifizierung,
Permoserstr. 15, D-04315 Leipzig, Germany,
Email: juergen.gerlach@iom-leipzig.de,
Tel.: +49 341 235 3310, Fax: +49 341 235 2313

[**)] now with Fraunhofer-Institut für Werkstoffmechanik (IWM), 06120 Halle/Saale, Germany

Introduction

Group III-nitrides are of great interest due to their numerous applications in optoelectronics as well as high-temperature and high-power devices. With its large direct bandgap width of 3.4 eV at room temperature, hexagonal gallium nitride, wurtzitic GaN (w-GaN), is a semiconducting material suitable for many applications in these areas. The most important ones are blue and white light emitting diodes, blue laser diodes, field-effect transistors and ultra-violet light sensors.[1-3] Conventional molecular beam epitaxy (MBE) has become an important synthesis method for deposition of GaN films because of its possibilities of in situ diagnostics and its potential of manufacturing more complex semiconductor components. A related method, ion-beam assisted MBE (IBA-MBE) that applies simultaneous low energy (hyperthermal) nitrogen ion irradiation of the growing GaN film, offers a number of respectable merits.[4] The importance of the influence of the Ga to N flux ratio during MBE growth has been an object of research for a long time and it is still, nowadays. In particular, the role of excess Ga during MBE growth of GaN was investigated in detail using in situ methods (see e.g. Ref. 5-8). Today, there is common agreement that with Ga-rich MBE growth conditions a Ga double layer (bilayer) is formed on the GaN surface in which the mobility of Ga atoms is much higher than on a pure GaN surface.[9] Only recently, time-dependent variations of MBE, like pulsed MBE,[10] metal modulated epitaxy (MME),[11] or migration enhanced epitaxy (MEE),[12,13] have been reported which are taking advantage of that higher Ga atom mobility under specified Ga-rich growth conditions. In all those time-modulated MBE variants the flux of reactive nitrogen is interrupted periodically, while the Ga flux remains constant, leading to highly mobile excess Ga adatoms. The resulting GaN films are characterized by a lower defect density and smoother surface compared to GaN films grown by conventional MBE.

The ultimate limit of Ga-rich growth as well as of time-modulated deposition is explored by completely separating the Ga deposition from the reaction of Ga with reactive nitrogen species, i.e. Ga is deposited first and afterwards post-nitridation of Ga takes place. Such an approach of separately delivered compound components is known as droplet epitaxy (DE),

as due to the low melting point of Ga (303 K) the deposited Ga is present on the substrate in form of liquid droplets.[14] In the case of GaN, DE is mainly applied for production of nano-dots or quantum-dots of low area density and narrow size distribution.[15-22] Most of the efforts were done for DE of GaN dots on Al_2O_3(0001), 6H-SiC(0001) and Si(111) substrates. Different variations of the DE method are known that differ in particular in the way how reactive nitrogen is supplied to the sample during the nitridation, e.g. reactive nitrogen from RF or ECR excited nitrogen plasmas,[16,18,20-22] atomic nitrogen from dissociation of NH_3,[17,19] atomic nitrogen from a NH_3 seeded supersonic jet source.[15]

However, the present study is not meant for producing nano-sized, well separated GaN dots by DE. In fact, here the total amount of deposited Ga atoms (see Table I) is several orders of magnitude larger than the ones typically used for quantum dot formation (10^{15} to 10^{16} Ga at. cm^{-2}) (see e.g. Ref. 15, 21). Secondly, the source of reactive nitrogen applied here is a sophisticated type of low-energy ion source that has been successfully used for IBA-MBE growth of GaN prior to this study (see e.g. Ref. 4, 23, 24). In this study, the method of ion-beam nitridation of Ga droplets is used to synthesize epitaxial GaN films on bare 6H-SiC(0001) substrates.

Experimental

Sample preparation was performed in a multi-chamber ultra-high vacuum (UHV) system for IBA-MBE which is described in detail in Ref. 25. GaN films were prepared in the deposition chamber (base pressure below 5×10^{-7} Pa) that is equipped with a conventional Ga effusion cell and a constricted glow-discharge (hollow-anode) nitrogen ion source. Ga was evaporated in an effusion cell temperature range from 970 to 1050 °C, corresponding to Ga deposition rates on the sample between 0.6×10^{14} and 2.2×10^{14} Ga at. $cm^{-2}s^{-1}$. The hollow-anode ion source, based on the principle of a constricted dc glow-discharge, was utilized to generate reactive N^+ and N_2^+ ions with a hyperthermal kinetic energy distribution not exceeding 25 eV.[23] These reactive nitrogen species contribute to the GaN formation,

while nitrogen molecules from the background gas with only thermal velocities can not. The binding energy of in a N_2 molecule is almost 10 eV, inhibiting the chemical reaction of Ga atoms with N_2 molecules. The nitrogen ion beam current density at the sample location was constant at a value of 25 µA cm^{-2}, equalling a nitrogen ion flux of 1.6×10^{14} ions $cm^{-2}\,s^{-1}$. The working pressure of 8×10^{-2} Pa originated from the N_2 gas flow of 12 standard cubic centimetres per minute (sccm) through the nitrogen ion source. The 6H-SiC(0001) substrates were ultrasonically cleaned using ethyl alcohol in order to degrease the surface, dried, and mounted on a Mo sample holder. Prior to growth, the substrates were heated in vacuum to 750 °C for 15 min of outgassing and then cooled down to the process temperature. It must be emphasized that in contrast to typical MBE of GaN, no nucleation or buffer layer of GaN or AlN was deposited. All GaN films of this study were formed directly on the bare 6H-SiC(0001) surface.

For every sample the Ga deposition time and substrate temperature were constant. In Tab. I the process parameters for all samples are listed. A two-step sequence was applied for the preparation of the GaN films (see Fig. 1):

(i) Ga deposition step: Ga was deposited onto the 6H-SiC(0001) substrate for a constant deposition time at different Ga deposition rates in a N_2 environment with a partial pressure that is equal to the working pressure of the nitrogen ion source. The ion source remained switched off during this process step. In order to obtain different total Ga coverages, the Ga deposition rate was varied for the samples.

(ii) Ion beam nitridation step: The Ga deposition flux was interrupted by closing the shutter of the Ga effusion cell and subsequently, the previously deposited Ga was irradiated with hyperthermal nitrogen ions from the hollow-anode ion source without any further Ga supply to form thin GaN films. The duration of irradiation t_{irr} corresponds to the deposited quantity of Ga and ranged between 30 and 140 min.

During both process steps, the substrate temperature was constantly 630 °C. It was chosen to be low enough to prevent thermal desorption of Ga, but also to be high enough, so that

GaN films of reasonably high quality could be synthesized. For comparison purposes, a reference sample (type R) was prepared without performing the nitridation step.

In situ reflection high-energy electron diffraction (RHEED) was used for monitoring the temporal evolution of the sample surface structure during the whole process. Measurements were conducted at an electron acceleration voltage of 30 kV and an incidence angle of about 2 deg to the substrate surface. In addition to taking snapshots of RHEED patterns, the reflected intensity was recorded throughout the process as a function of time. The surface topography of the prepared films was investigated by scanning electron microscopy (SEM). High-resolution x-ray diffraction (XRD) and x-ray texture goniometry with collimated Cu $K\alpha_1$ radiation (λ = 0.15406 nm) were used to examine the crystallographic structure and texture of the films, respectively. Monochromatization was achieved with a double-crystal Ge(220) monochromator in the (+,-) arrangement. The same setup was applied for x-ray reflectivity (XRR) measurements in order to determine the average film thickness. Reflectivity curve modeling was done with the commercially available software RayfleX. Information on the stoichiometry, as well as on the defect structure of the films was obtained by Rutherford backscattering spectrometry (RBS) and ion channelling (RBS/C). The measurements were performed at the ion accelerator facility of the University of Leipzig with a 2 MeV He^+ analysis ion beam with the backscattered ions detected at an angle of 170 deg. For RBS data analysis the computer code RUMP was applied.[26] A selected sample was examined with high-resolution, cross-section transmission electron microscopy (TEM) in a 400 kV electron microscope at a point resolution of 0.155 nm. The TEM sample preparation comprised face-to-face gluing, cutting, plane-parallel grinding and polishing, one-sided dimpling, and both sided Ar^+-beam etching at 3 keV under an incidence angle of 5 deg. Eventually, to reduce sample charging during the TEM analysis, a selective carbon coating process was applied (for details see Ref. 27).

Results

Five types of GaN samples were deposited on 6H-SiC(0001) substrates at variation of the Ga flux j_{Ga} and the related duration t_{irr} of the N ion bombardment (see Fig. 1). All other parameters, substrate temperature T_{sub}, nitrogen ion flux j_N , particle energies E_{Ga} and E_N and the deposition time t_{dep} remained constant (see Tab. I).

The Ga deposition flux was chosen in such a way that the total amount of deposited Ga would correspond to a several nanometers thick layer, albeit it should be noticed that the assumption of a Ga layer with homogeneous thickness is by no means valid (as will be shown later).

The surface arrangement and surface crystallinity of the formed material were obtained by RHEED measurements. The set of patterns in Fig. 2 shows the time-resolved RHEED investigation exemplary for the sample of type A that allows tracking of the evolution of the sample surface structure with time. The image underneath (Fig. 2a) is a diagram of the diffracted electron beam intensity throughout the procedure. The set of RHEED patterns begins with the typical diffraction spots expected for the pristine 6H-SiC(0001) surface (Fig. 2b). As soon as the Ga deposition step begins (t = 0 min), the recorded RHEED reflection intensity in Fig. 2a decreases. After 30 min of Ga exposure the initial substrate RHEED pattern has vanished completely. Instead, the RHEED pattern (Fig. 2c) now indicates an amorphous-like state of the surface, as the substrate surface is covered with disordered (liquid) Ga sufficiently enough to prevent electrons to be reflected from the substrate surface itself. At that point (after 30 min) the Ga deposition flux was stopped by closing the effusion cell shutter. The start of the ion beam nitridation step (t = 30 min) causes a restoration of the RHEED reflection intensity until it saturates at about 30 min of nitridation time (Fig. 2a). A closer examination of the RHEED patterns during the nitridation step shows that after a short incubation time (3 min of nitridation, Fig. 2d), weak diffraction spots appear that cannot be related to 6H-SiC anymore but to twinned zinc-blende GaN (see Ref. 25,28). The spotty character of the RHEED pattern resembles such of typical GaN nano-dots as reported by other groups.[16,20,22] This marks the detectable onset of epitaxial GaN growth on the substrate surface. In the further course of the N ion beam nitridation process, the RHEED

pattern intensity increases and diffraction streaks appear in addition to the spots (Fig. 2f). A detailed analysis of the RHEED patterns indicates that the GaN film on the substrate consists of a mixture of both the stable hexagonal polytype, wurtzitic GaN (w-GaN), and the metastable cubic polytype, zinc-blende GaN (z-GaN),[25,28] but w-GaN is predominant, here. The final stage after stopping the nitrogen ion flux (Fig. 2g) shows a distinguishable streaky pattern. This is an indication of a smoothening of the film surface. SEM measurements confirm the RHEED patterns in that respect (see below). Obviously, according to the RHEED results the deposited Ga, being liquid at the used substrate temperature, was transformed into epitaxial GaN during the nitrogen ion irradiation step.

To study the initial arrangement of the Ga deposited on the 6H-SiC(0001) substrate, one substrate was exposed to Ga at exactly the same Ga deposition rate and deposition time as sample A. Afterwards, this reference sample (type R) was not nitridated, but cooled to room temperature, removed from the deposition system and investigated with SEM. The SEM image of that sample in Fig. 3a shows an arrangement of Ga droplets with a diameter of up to 250 nm randomly distributed on the substrate surface. Obviously, the relatively high substrate temperature of 630 °C at the Ga deposition resulted in a high surface mobility of Ga adatoms. In Fig. 3b the same type of sample is shown after the ion beam nitridation step (type A). The two SEM images clearly demonstrate that the initial Ga droplets were transformed into a GaN film with a mosaic-like morphology consisting of strongly coagulated GaN domains (see Fig. 3b). The topography of the film resembles that of typical GaN films grown by MBE, except for distinct remains of unfinished coalescence in form of canyons and holes. It should be noted that a distinct degree of lateral growth is a prerequisite for the obtained transformation of isolated Ga droplets in an almost compact GaN thin film. Furthermore, the SEM micrograph of the final GaN film in Fig. 3b does hardly exhibit any hints at how the initial size and arrangement of Ga droplets may have been. The topography of the GaN domains appears rather smooth, as was already indicated by the streaky RHEED pattern in Fig. 2g. Further evidence is given by Fig. 4a and 4b which depict results of XRR measurements for two samples of types A and D, respectively. The intense oscillations

indicate high thickness homogeneity. The measured reflectivity curves are overlaid with simulated reflectivity curves. On this base, the GaN film thickness could be calculated to 29 nm (A) and 93 nm (D) with a surface roughness between 1.5 and 2 nm. By regression analysis a linear correlation between the film thickness determined by XRR and the Ga area density derived from RBS spectra (see below) in Fig. 4c was obtained. (The area density indicated is not to be confused with the actual volume density of the sample.) According to these measurements, no loss of Ga did occur during the deposition and nitridation processes. Thus, all the deposited Ga atoms are eventually part of the formed GaN film.

Applying RBS under random and channeling conditions with a 2.0 MeV He^+ beam, the depth distribution of defects and layer interfaces were investigated. In Fig. 5, the random RBS measurement (blue line) of the GaN film with the largest thickness in this study of 90 nm (sample type D) is shown together with the corresponding simulated RBS spectrum (red line) and with the ion channeling spectrum (green line). The slopes of the Ga-related signal in the random measurement are very steep and the lower energy slope fits very well with the slope of the Si-related signal from the SiC substrate indicating a sharp GaN to SiC interface. The slightly poor match in the low energy region after the carbon peak can be attributed to detector noise in this energy range. The simulation of the random measurement reveals a 1:1 stoichiometry of Ga and N in the film. Ion channeling was done with the alignment of the analysis beam along the c-axis of the GaN film. The small peak at ~1.58 MeV in the channeling spectrum can be identified as the surface peak that is typical for such type of measurements due to backscattering of He^+ projectiles at surface atoms of the film. When sensing deeper into the film, the signal intensity of the aligned spectrum increases significantly. This is related to an increasing defect density when approaching the substrate surface. The minimum backscattering yield χ_{min} is found to be about 15%. This value is high in comparison with the 1 to 2% that is usually measured for GaN films of the highest crystalline quality.[24] It originates from defects in the film like the already observed mixture of polytypes. Nonetheless, the defect density in the GaN film is still at a level that is low enough to allow for significant channeling of He ions within the 6H-SiC substrate.

GaN usually crystallizes in two types of crystal structures: a metastable cubic (zinc-blende) GaN structure and a stable hexagonal (wurtzite) GaN structure. The hexagonal GaN is commonly grown on the basal plane of 6H-SiC at temperatures > 700 °C. The RHEED measurements have shown that the crystalline and epitaxial GaN films formed by the ion-beam nitridation process consist of hexagonal and cubic GaN polytype fractions (w-GaN and z-GaN, respectively). To distinguish between them, x-ray texture measurements were performed. In Fig. 6 the hexagonal $\{10\bar{1}1\}$ and the cubic {200} XRD pole figure of a typical GaN film (sample A, thickness 29 nm) containing both polytypes is shown. From the fact that distinct, separated and narrow pole density maxima are visible, it can be concluded that the film is of high crystalline order. The number of pole density maxima in the cubic pole figure reveals that the cubic phase appears in two-fold form in the film. The existence of a second set of three pole density maxima, rotated against the first set by 180 deg, proves the existence of cubic rotational twins. This is a well-known phenomenon at growth of thin GaN films.[29] The epitaxial relationships between hexagonal and cubic polytypes, as derived from the pole figures, are w-GaN(0001) || z-GaN(111) and w-GaN$[2\bar{1}\bar{1}0]$ || z-GaN$[\bar{1}10]$ or z-GaN$[1\bar{1}0]$, proving the findings from the *in situ* investigations by RHEED (see Fig. 2).

As it is not feasible to derive directly from the texture measurements, where the z-GaN polytype fraction is actually located within the GaN film, TEM analysis of a cross-sectionally prepared sample was performed. A typical low-magnification TEM bright field micrograph of a defective GaN film formed by nitrogen ion bombardment of Ga droplets at 630 °C of type D is shown in Fig. 7a. The morphology is dominated by stacking defects parallel to the SiC substrate surface and threading defects extending away from the substrate. The surface is smooth at this magnification. A TEM micrograph of the GaN film at high-resolution is shown in Fig. 7b. The GaN film consists of an about 10 nm thick zinc-blende GaN layer (z-GaN) followed by a thick layer of wurtzite GaN (w-GaN). The triangular, material-free structures (voids) at the interface in the z-GaN film (arrows) are an interesting aspect and can be explained with the model presented in the next chapter. The high-resolution micrograph of the z-GaN/6H-SiC interface region in Fig. 7c exhibits the very smooth interface between the

z-GaN layer and the w-GaN layer. The transition from z-GaN to w-GaN is abrupt within one monolayer. The micrograph taken from a region near to the surface of the w-GaN layer (Fig. 7d) shows an atomically almost perfect structure between the defects. The selected area electron diffraction (SAED) pattern in Fig. 7e indicates a superposition of 6H-SiC and w-GaN diffraction patterns, confirming epitaxial growth. Extra diffraction spots are also visible, which can be indexed as originating from the zinc-blende polytype of GaN, and streaking due to the stacking disorder is also apparent. Thin films under ion bombardment exhibit mechanical residual stress, which can be tensile as well as compressive, depending on irradiation parameters and substrate temperature (details see e.g. Ref. 30). It is assumed that at the beginning of the GaN layer formation the ion-induced compressive stress and densification are so high and the film thickness so small that probably no stacking faults can be generated. A thin layer of the metastable zinc-blende GaN phase is formed. With increasing film thickness, the lower energy of the wurtzite structure makes it energetically favourable to introduce stacking faults in the zinc-blende films, whereby switching to the wurtzite structure.[31]

Discussion

Summarizing the investigations, it can be stated that the hyperthermal ion beam nitridation of liquid Ga droplets on a single crystalline substrate at elevated substrate temperature results in a relatively continuous epitaxial GaN film of reasonable thickness homogeneity. The GaN film consists of coalesced large domains that are almost free of defects. Characteristic for the underlying growth mechanism is the evident presence of a high degree of lateral growth in combination with large diffusion lengths.

Based upon above experimental results, it can be assumed that the liquid Ga droplet surface represents a significant mass transport path. The deposited nitrogen on the liquid Ga surface can diffuse along the surface to peripheral regions of the liquid-solid interface, driven by both the decrease in the surface energy and the concentration gradient. This interface acts as a sink for nitrogen particles dissolved on the drop. The surface diffusion process to

the peripheral region is followed by a liquid-solid interfacial diffusion and a crystallization process from the peripheral region towards the centre of the interface. In summary, the evolution of the surface is driven by the tendency of the system to lower its free energy or chemical potential.

In this mechanism to form a thin GaN film (shown in Fig. 8) four consecutive steps are involved:

(a) Deposition: the mass transport of atomic and molecular nitrogen ions in the vapour phase to the vapour-liquid and the vapour-solid (substrate) interface; the desorption from the droplet and substrate surface is rather small;

(b) Diffusion: the diffusion of the nitrogen atoms and dissociated molecular ions at the droplet surface and also on the surface of the substrate to the peripheral region;

(c) Nucleation and growth: two-dimensional nucleation and beginning growth of crystalline GaN seeds at the liquid-solid contact point (peripheral region);

(d) Growth stop: the formation of the crystalline GaN islands to a closed film by coalescence.

In this process, the liquid metallic nanodroplets after Ga deposition must be stable. The stability of such a liquid droplet of radius *R* in its own vapour depends on the degree of supersaturation Σ. The minimum critical radius is given by the well-known Gibbs-Thomson equation [32] (also known as Thomson-Freundlich equation [33]) to

$$R_{\min} = \frac{2\Omega_l}{k_B T} \frac{\gamma_{vl}}{\ln \Sigma}, \qquad (1)$$

where Ω_l is the liquid atom volume, k_B is the Boltzmann constant and γ_{vl} is the liquid-vapour interface energy.[32] By variation of the supersaturation and/or of the substrate temperature the radius of Ga droplets can be controlled.

In principle, the hyperthermal nitrogen ion irradiation (< 25 eV) of the substrate surface covered with liquid Ga droplets can be described as a soft-landing process of nitrogen ions. This is characterized on the one hand by negligible surface damage,[24] but on the other hand by a high energy of the nitrogen atoms on the surface in comparison with the thermal energy

of the particles at conventional vapour deposition (typically 0.2…0.4 eV). The adsorbed nitrogen covers the surface and is not incorporated into the liquid Ga. It can be assumed that the high substrate temperature (here: 630 °C) and the curved surface of the droplets induce a fast diffusion of active nitrogen species and the growth of a crystalline GaN film preferred at the perimeter of the liquid-solid interface (see Fig. 9). Consequently, the individual processes of the nitrogen mass transport must be considered in detail:

(i) Mass transport by diffusion through the liquid droplet

A concentration gradient from the vapour-liquid interface to the liquid-solid interface is needed for the bulk liquid diffusion with a discernible nitrogen current J_d. But the solubility of nitrogen in liquid Ga can be neglected for the substrate temperature applied here.[34] With that, the diffusion of nitrogen through liquid Ga droplets is also extremely low (i.e. $J_d \approx 0$). It should be noted that bulk liquid diffusion coefficients can be expected which are smaller than 10^{-5} cm² s^{-1}. Moreover, epitaxial GaN formation from inside the Ga droplet at the substrate surface immediately below the droplet would contradict the observed RHEED pattern evolution during the nitridation process.

(ii) Mass transport by diffusion at the vapour-solid interface

It is known that the surface diffusion coefficient of atoms diffusing on a solid surface at higher temperatures and particularly on a liquid surface is several orders of magnitude higher in comparison to the diffusion through a bulk liquid, because much longer jump distances can be assumed,[35] or cooperative motion in which large numbers of surface atoms take part is suggested.[36] The current on the flat substrate surface J_{ss} is empirically related to the surface concentration C_s by Fick´s law

$$J_{SS} = -D_{SiC}\frac{\partial C_N}{\partial x}\ , \quad \text{where} \quad D_{SiC} = \frac{1}{4}\lambda_0^2 \nu \cdot \exp\left(-\frac{E_m}{k_B T}\right) \tag{2}$$

and D_{SiC} is the diffusion coefficient of nitrogen on the SiC surface, λ_o is the mean square displacement of an atom in one dimension (≈ lattice constant, a = 0.30806 nm for 6H-SiC), ν is the frequency of oscillations of an atom at the substrate surface (≈10^{13} s^{-1}) and E_m is the activation energy of diffusion. The denominator 1/4 in Eq. (2) comes from the assumption

that the substrate has a simple square lattice on the surface. At the applied temperature of 630 °C and an activation energy E_m > 1 eV the pre-exponential factor is unity and the diffusion coefficient D_{SiC} can be estimated to be about 2.5 × 10^{-3} cm² s^{-1}. Consequently, this lateral diffusion process must be taken into account. As a matter of fact, this diffusion mechanism is also inherent in conventional MBE growth of GaN films.

(iii) Mass transport by diffusion on the surface of the liquid Ga droplet

An additional pathway for reactive nitrogen species to travel toward the perimeter between the liquid droplet and the solid surface along the droplet surface must be taken into account. If a macroscopic current of particles on the surface, represented by $J_{cs}(x,t)$ is considered, then the surface diffusion can be described by the continuity equation,[37] because diffusion conserves the total number of particles on the surface. The surface current is related to the gradient of the chemical potential, $J_{cs}(x,t) \propto -\nabla\mu(x,t)$, because the surface current will flow from regions of higher chemical potential to areas of lower potential. Consequently, this potential is related to the number of bonds that must be broken by an atom to diffuse. Surface areas that have a positive (convex) curvature have more available bonds than areas with negative (concave) curvature, i.e. an atom can diffuse more readily. This curvature dependence can be approximately expressed in terms of the curvature $\partial^2 h/\partial x^2$, since $|\partial h/\partial x| << 1$ and is given by the Gibbs-Thomson relationship [38]

$$\mu = \mu_0 - \gamma\Omega\frac{\partial^2 h}{\partial x^2} \qquad \text{or} \qquad \frac{\partial\mu}{\partial x} = -\frac{\partial h}{\partial x}\left(\gamma\Omega\frac{\partial^2 h}{\partial x^2}\right) = -\gamma\Omega\frac{\partial^3 h}{\partial x^3} \tag{3}$$

where μ and μ_0 are chemical potentials of the curved and flat surfaces, respectively, γ is the surface energy, Ω is the nitrogen atomic volume and $\nabla\mu_0 = 0$ on the flat surface. The gradient of chemical potential generates the surface current J_{cs} given with the Nernst-Einstein term to

$$J_{CS} = -N_S\left(\frac{D_S^{lGa}}{k_B T}\right)\frac{\partial\mu}{\partial x} = N_S\frac{D_S^{lGa}}{k_B T}\gamma\Omega\frac{\partial^3 h}{\partial x^3}, \tag{4}$$

where N_s is the average areal density or number of atoms per unit area, D_s^{lGa} is the diffusion coefficient of nitrogen on the liquid Ga surface and k_B the Boltzmann constant linking this

potential driving force with the flux. That means that the driving force, such as the gradient in concentration, can be reduced to a chemical potential and their effect on the flux can be expressed by this equation. Contrary to the consideration of diffusion within the liquid Ga droplet (see above), the diffusion coefficients on liquid surfaces vary in the range between 10^{-4} to 1 cm² s^{-1} only,[39] where the surface energy of the liquid Ga is assumed to be between the half and a third of the surface energy of solid Ga (= 2.82 eV [40]). It can be stated that the nitrogen diffusion coefficient on the liquid Ga surface is larger than on the flat SiC surface and the nitrogen current J_{cs} on the curved liquid Ga surface is strongly increased because $J_{cs} \propto \nabla^3 h$.

Combining equations (3) and (4), the well-known Mullins equation [41] is given by

$$\frac{\partial h(x,t)}{\partial t} = -\Omega \frac{\partial h}{\partial x}\left\{-\left(N_S \frac{D_S^{lGa}}{k_B T}\right)\left[-\frac{\partial h}{\partial x}\left(\gamma\Omega \frac{\partial^2 h}{\partial x^2}\right)\right]\right\} = -B\nabla^4 h \qquad (5)$$

where $B = N_S \frac{D_S^{lGa}}{k_B T}\gamma\Omega^2$. Consequently, the depletion of the droplet is proportional to $\nabla^4 h$ caused by an accelerated diffusion on the curved surface in direction of the perimeter at the solid-liquid interface. The directional diffusion over the surface of the liquid Ga droplet is probably the preferential diffusion path in the process investigated here.

(iv) Mass transport by low-energy nitrogen ion sputtering of the liquid Ga surface

When the energy of the incident energetic projectiles (here atomic and molecular nitrogen ions with energies of up to 25 eV) overcome the surface binding energy, then a sputter erosion of the liquid Ga droplets can be expected. Experimentally, a pronounced temperature dependence is observed in the sputtering yield for higher temperatures.[42] Sigmund has concluded that the sputter behaviour of liquids strongly depends on the surface binding energy (surface tension in case of liquids).[43] The corresponding current of sputtered atoms J_{sp} can be expressed as

$$J_{sp} = Y \frac{J_I t}{N_S} \qquad (6)$$

in terms of the sputtering yield Y, the ion current density J_I and the sputter time t. The sputtering yield is increased by reduction of the surface binding energy. The change in this energy with temperature must be taken into account and included in the sputtering yield calculation. The temperature dependence of the surface energy can be fitted by certain empirical expressions, e.g. proposed by van der Waals,[44]

$$\gamma_{vl}(T) = \gamma_{vl,0}\left(1-\frac{T}{T_C}\right)^{1+n} \qquad (7)$$

where $\gamma_{vl,o}$ ist the surface energy at the melting point (here for Ga at 305 K is $\gamma_{vl,o}$ = 2.83 eV [40]), T_c is the conjugate temperature (here T_c = 5419 K,[40] details see Ref. 45) and the fit parameter n = 2/9.[46]

Based upon above considerations, the sputtering yield of liquid Ga at 25 eV nitrogen ion bombardment was calculated. According to models by Bohdansky et al. [47] and Yamamura and Tawara [48] and with $\gamma_{vl}(T)$ = 2.55 eV, the sputtering yields at 630 °C were 0.05 and 0.04 atoms per ion respectively. Consequently, the influence of nitrogen ion sputtering can be neglected. This is in agreement with the experimental results presented in the first section of this study.

Contributions to the surface atomic current on the liquid droplet by momentum transfer from the incident ions to atoms on the surface, which is proposed by Carter and Vishnyakov as well as by Moseler et al.,[49,50] are not considered, because momentum transfer at the used ion energies (< 25 eV) seems to be too low.

Summarizing all considerations of this section, diffusion along the liquid Ga droplet surface towards the liquid-solid interface should be the most favourable mass transport path of reactive nitrogen species, the diffusion along the surface of the substrate and of the already formed GaN the second favourable. Studies have shown, that lateral growth proceeds via a reactive spreading mechanism including an approximately 2 ML thick metallic wetting layer fed by outdiffusion of the metal from the droplets.[51] Regarding the mass transport of Ga in the present study, it can be assumed that the pronounced lateral growth observed here is based on the same mechanism. Characteristic for the discussed GaN film

formation process is the presence of voids in the GaN film (see Figs. 7b and 8d) which are situated directly at the substrate surface. At these locations, adjacent GaN crystallites coalesced and formed voids. The presence of interfacial voids is untypical for MBE grown GaN films. Instead, it is a direct consequence of the two dominating nitrogen diffusion paths. Filling of the voids is prevented during the further GaN growth, as the nitrogen diffusion flux is blocked by coalesced GaN domains.

Conclusions

Thin GaN films of different thicknesses of up to 90 nm were synthesized on 6H-SiC(0001) substrates by using ion-beam nitridation epitaxy, i.e. by Ga deposition and post-nitridation with hyperthermal nitrogen ions. Upon this, the initially formed liquid Ga droplets are transformed into a coalesced GaN film of low surface roughness and high crystalline quality. The results demonstrate that diffusion is playing a main role in this process. Possible diffusion paths of reactive nitrogen species are discussed and it is concluded that surface diffusion on the Ga droplet surface towards the Ga droplet perimeter and the lateral diffusion along the substrate surface as well as on the already formed GaN film are the most probable diffusion mechanisms. Due to the curvature of the Ga droplets the diffusion is expected to be strongly enhanced by curvature dependent diffusion.

Apart from the approach to form GaN films by transformation of Ga droplets to a heteroepitaxial GaN film as applied here, the observations and related considerations are also valid for the Ga-rich MBE and IBA-MBE growth of GaN films in presence of Ga droplets on the sample surface. There, the Ga droplets themselves act as an additional source for the secondary formation of homoepitaxial GaN. Contrary, remaining Ga droplets after Ga-rich growth of GaN films by MBE and IBA-MBE, that are mostly of a disturbing character, can be entirely converted into epitaxial GaN by the described nitridation process. Afterwards, no excess Ga will be present on the sample, anymore, allowing for virtually unimpeded further processing of the sample.

This technique could be an alternative approach to prepare thin epitaxial GaN films with a high crystalline quality.

Acknowledgments

The authors thank Dr. A. Anders (Lawrence Berkeley National Laboratory, Berkeley, US) for providing the hollow-anode ion source, D. Hiller (Universität Freiburg, Germany) and Dr. C. Patzig (IWM Halle/S.; Germany) for the assistance in the early stages of this study, and Prof. T. Butz and Dr. J. Vogt (Universität Leipzig, Germany) for providing access to the Leipzig ion accelerator facility. Prof. S. G. Mayr (IOM Leipzig, Germany) is acknowledged for asking the right questions upon proofreading. This study was partially funded by the Deutsche Forschungsgemeinschaft (DFG) as part of the German Excellency Initiative in the Graduate School BuildMoNa (Universität Leipzig, Germany).

References

(1) Hangleiter, A. *MRS Bulletin* **2003**, *28*, 350.

(2) Pearton, S. J.; Abernathy, C. R.; Ren, F. Barabási, A.-L.; Stanley, H. E. *Gallium nitride processing for electronics, sensors and spintronics (engineering materials and processes)*; Springer: London, 2006.

(3) Takahashi, K.; Yoshikawa, A.; Sandhu, A.; Eds.; *Wide bandgap semiconductors: fundamental properties and modern photonic and electronic devices*; Springer: Berlin-Heidelberg, 2007.

(4) Sienz, S.; Gerlach, J. W.; Höche, T.; Sidorenko, A.; Mayerhöfer, T. G.; Benndorf G.; Rauschenbach, B. *J. Cryst. Growth* **2004**, *264*, 184.

(5) Held, R.; Crawford, D. E.; Johnston, A. M.; Dabiran, A. M.; Cohen, P. I. *Surf. Rev. Lett.* **1998**, *5*, 913.

(6) Heying, B.; Averbeck, R.; Chen, L. F.; Haus, E.; Riechert, H.; Speck, J. S. *J. Appl. Phys.* **2000**, *88*, 1855.

(7) Pavlovska, A.; Bauer, E. *Surf. Sci.* **2001**, *480*, 128.

(8) Pavlovska, A.; Bauer, E.; Smith, D. J. *Surf. Sci.*, **2002**, *496*, 160.

(9) Northrup, J. E.; Neugebauer, J.; Feenstra, R. M.; Smith, A. R. *Phys. Rev. B* **2000**, *61*, 9932.

(10) Mei, F.; Fu, Q. M.; Peng, T.; Liu, C.; Peng, M. Z.; Zhou, J. M. *J. Appl. Phys.* **2008**, *103*, 094502.

(11) Moseley, M.; Billingsey, D.; Henderson, W.; Trybus, E.; Doolittle, A. *J. Appl. Phys.* **2009**, *106*, 014905.

(12) Kawaharazuka, A.; Yoshizaki, T.; Hiratsuka, T.; Horikoshi, Y. *Phys. Status Solidi C* **2010**, *7*, 342.

(13) Wong, Y.-Y.; Chang, E. Y.; Wu, Y.-H.; Hudait, M. K.; Yang, T.-H.; Chang, J.-R.; Ku, J.-T.; Chou, W.-C.; Chen, C.-Y.; Maa, J.-S.; Lin, Y.-C. *Thin Solid Films* **2011**, *519*, 6208.

(14) Koguchi, N.; Ishige, K. *Jap. J. Appl. Phys.* **1993**, *32*, 2052.

(15) Hu, C.-W.; Bell, A.; Shi, L.; Ponce, F. A.; Smith, D. J.; Tsong, I. S. T. *Appl. Phys. Lett.* **2003**, *82*, 2889.

(16) Wu, C.-L.; Chou, L.-J.; Gwo, S. *Appl. Phys. Lett.* **2004**, *85*, 2071.

(17) Gherasimova, M.; Cui, G.; Jeon, S.-R.; Ren, Z.; Martos, D.; Han, J. *Appl. Phys. Lett.* **2004**, *85*, 2346.

(18) Kondo, T.; Saitoh, K.; Yamamoto, Y.; Maruyama, T.; Naritsuka, S. *Phys. Status Solidi A* **2006**, *203*, 1700.

(19) Maruyama, T.; Otsubo, H. Kondo, T.; Yamamoto, Y.; Naritsuka, S. *J. Cryst. Growth* **2007**, *301-302*, 486.

(20) Wang, Y.; Özcan, A. S.; Sanborn, C.; Ludwig, K. F.; Bhattacharyya, A.; Chandrasekaran, R.; Moustakas, T. D.; Zhou, L.; Smith, D. J. *J. Appl. Phys.* **2007**, *102*, 073522.

(21) Debnath, R. K.; Stoica, T.; Besmehn, A.; Jeganathan, K.; Sutter, E.; Meijers, R.; Lüth, H.; Calarco, R. *J. Cryst. Growth* **2009**, *311*, 3389.

(22) Schupp, T.; Neuschl, B.; Meisch, T.; Feneberg, M.; Thonke, K.; Lischka, K.; As, D. J.; *J. Cryst. Growth* **2010**, *312*, 3235.

(23) Anders, A.; Newman, N.; Rubin, M.; Dickinson, M.; Jones, E.; Phatak, P.; Gassmann, A. *Rev. Sci. Instrum.* **1996**, *67*, 905.

(24) Gerlach, J. W.; Schwertberger, R.; Schrupp, D.; Sienz, S.; Attenberger, W.; Rauschenbach, B. *IPAP Conf. Ser.* 2000, 1, 202.

(25) Neumann, L.; Gerlach, J.W.; Rauschenbach, B.; submitted to *Thin Solid Films*.

(26) Doolittle, L. R. *Nucl. Instrum. Meth. B* **1986**, *15*, 227.

(27) Höche, Th.; Gerlach, J. W.; Petsch, T. *Ultramicroscopy* **2006**, *106*, 981.

(28) Honda, T.; Fujita, N.; Maki, K.; Yamamoto, Y.; Kawanishi, H. *J. Cryst. Growth* **2000**, *209*, 392.

(29) Gerlach, J. W.; Sienz, S.; Attenberger, W.; Rauschenbach B. *Physica B* **2001**, *308-310*, 81.

(30) Davis, C. A. *Thin Solid Films* **1993**, *226*, 30.

(31) Strite, S.; Lin, M. E., Morkoc, H. *Thin Solid Films* **1993**, *231*, 197.

(32) Thomson W. *Phil. Mag.* **1871**, 43. Gibbs, J. W. *Trans Connect. Acad.* **1876**, *3*, 108.

(33) Freundlich, H. In *Fortschritte der Kolloidchemie*; Steinkopf: Dresden, 1926.

(34) Egelstaff, P. A. *An introduction to the liquid state*; Clarendon: Oxford, 1992.

(35) Delmare, F.; Read, G. E. *Surf. Sci.* **1971**, *28*, 267.

(36) Bhin, V. T.; Melinon, P. *Surf. Sci.* **1985**, *16*, 234.

(37) Barabási, A.-L.; Stanley, H. E. *Fractal concepts in surface growth*; Cambridge University Press: New York, 1995.

(38) Noziéres, P. In *Solids far from equilibrium*; Godréche, C., Ed.; Cambridge University Press: Cambridge, 1991; p. 1-154.

(39) Bonzel, H. P. In *Surface mobilities on solid materials, fundamental concepts and application*; Bhien, V. T., Ed.; Plenum Press: New York, 1983; p. 195-241.

(40) Grossman, A.; Doerner, R. P.; Luckhardt, S. *J. Nucl. Mater.* **2001**, *290-293*, 80.

(41) Mullins, W. W. *J. Appl. Phys.* **1957**, *28*, 333.

(42) Besocke, K.; Berger, S.; Hofer, W. O.; Littmark, U. *Rad. Eff.* **1982**, *66*, 35.

(43) Sigmund, P. *Phys. Rev.* **1969**, *184*, 383.

(44) Van der Waals, J. D. *Z. Phys. Chemie.* **1894**, *13*, 716.

(45) Cahn, J. W.; Hillard, J. E. *J. Chem. Phys.* **1958**, *28*, 258.

(46) Guggenheim, E. A. *J. Chem. Phys.* **1945**, *13*, 253.

(47) Bohdansky, J.; Roth, J.; Bay, H. L. *J. Appl. Phys.* **1980**, *51*, 2861.

(48) Yamamura, Y.; Tawara, H. *Atomic Data and Nucl. Tables* **1996**, *62*, 149.

(49) Carter, G.; Vishnyakov V., *Phys. Rev. B* **1996**, *54*, 17647.

(50) Moseler, M.; Gumbsch, P.; Casiraghi, C.; Ferrari, A. C.; Robertson, J. *Science* **2005**, *309*, 1545.

(51) Sidorenko, A.; Peisert, H.; Neumann, H.; Chassé, T. J. Surf. *Sci.* **2007**, *601*, 4521.

Tables

Tab. I: Deposition parameters and characteristic values of the GaN films.

Sample type	Effusion cell temperature [°C]	Ga deposition rate [at. cm^{-2} s^{-1}]	Deposition time [s]	Total Ga coverage [at. cm^{-2}]	Calculated average GaN coverage θ		Film thickness (XRR) [nm]	z-GaN present
					[nm]	[ML]		
A	970	0.7×10^{14}	1800	1.3×10^{17}	29	112	29	✓
B	1000	1.0×10^{14}	1800	1.8×10^{17}	41	158	40	✓
C	1020	1.4×10^{14}	1800	2.5×10^{17}	57	220	59	✓
D	1050	2.2×10^{14}	1800	4.0×10^{17}	90	347	93	✓
R	970	0.7×10^{14}	1800	1.3×10^{17}	-	-	-	-

Figures

Fig. 1: Experimental step sequence and parameters.

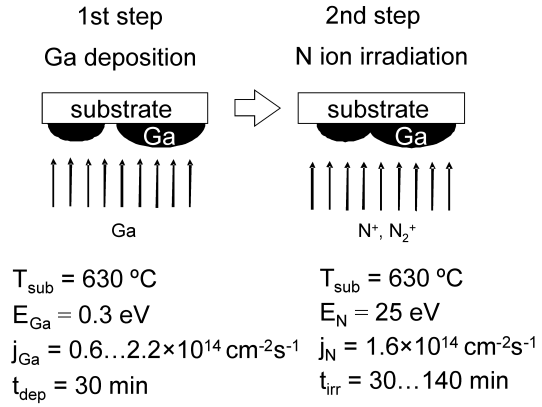

Fig. 2: In-situ RHEED investigation on a sample of type A.

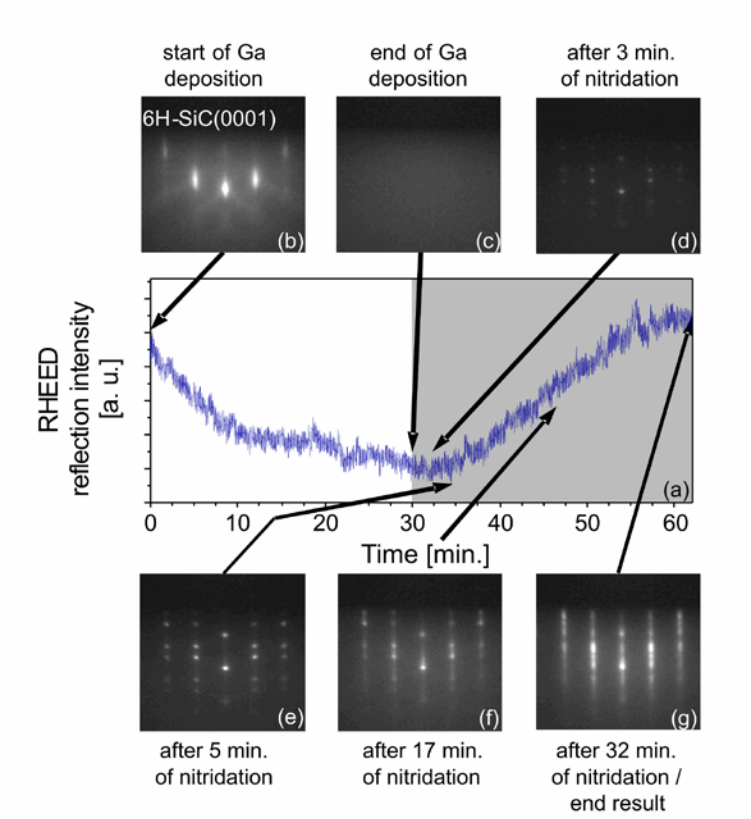

Fig. 3: SEM images of Ga droplets on the 6H-SiC(0001) substrate after 30 min of Ga deposition at 630 °C (a) and the highly coagulated GaN film obtained after N ion beam irradiation of such Ga droplets at the same temperature (b).

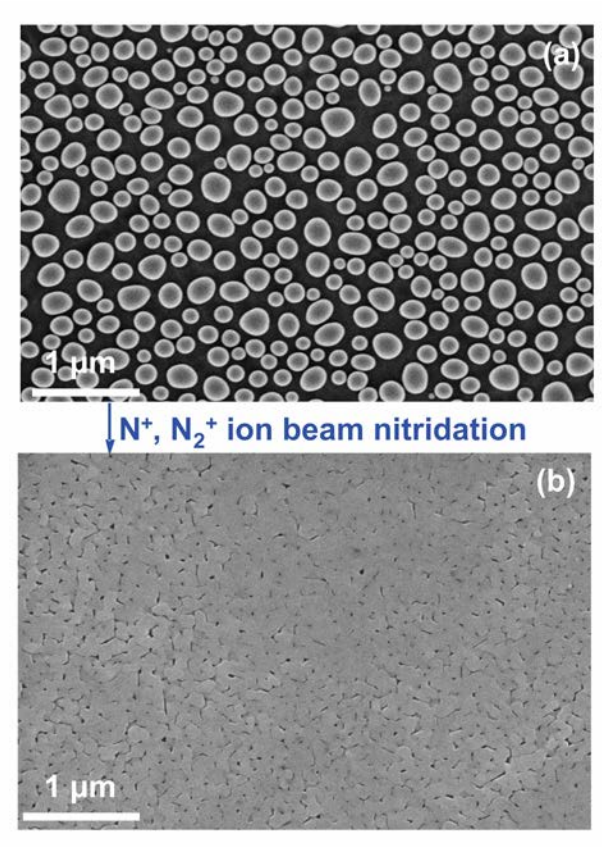

Fig. 4: XRR measurements of two samples of type A (thinnest) and D (thickest) (a and b), as well as the GaN film thickness derived from XRR as a function of the amount of Ga atoms deposited prior to the nitridation step (c).

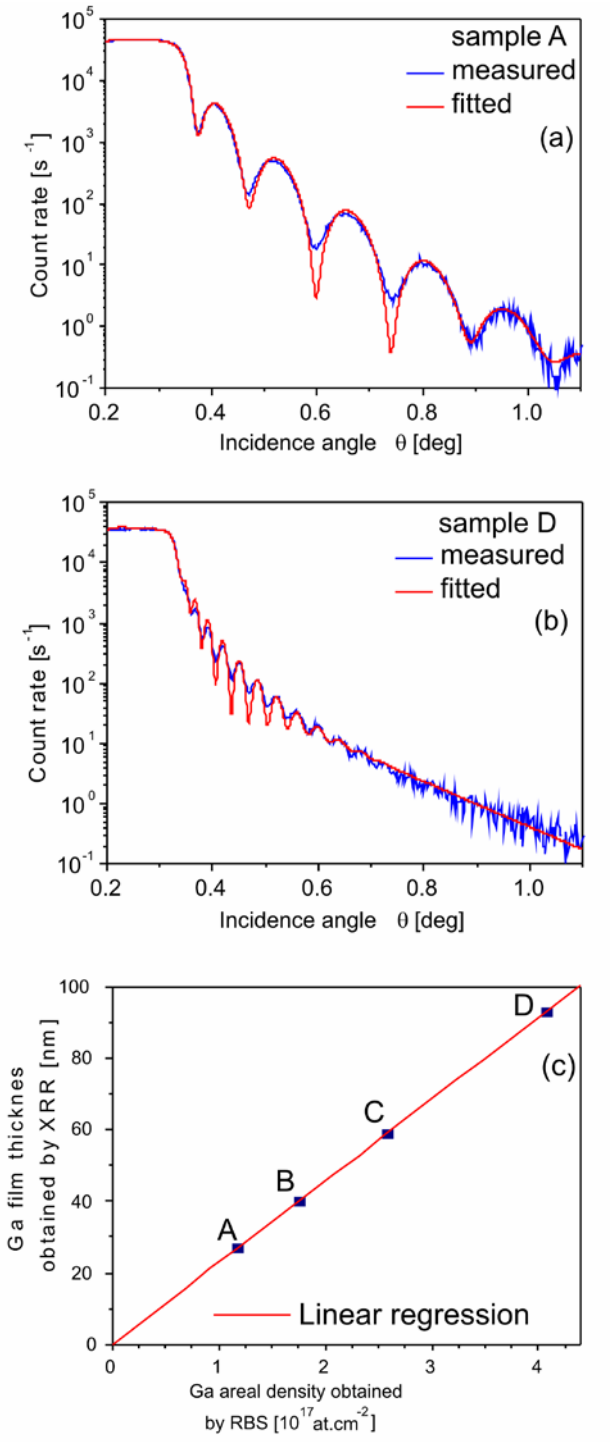

Fig. 5: Random (black), channeling (green) and fitted (red) RBS spectra of a 90 nm thick GaN film on SiC substrate prepared under the conditions of type D.

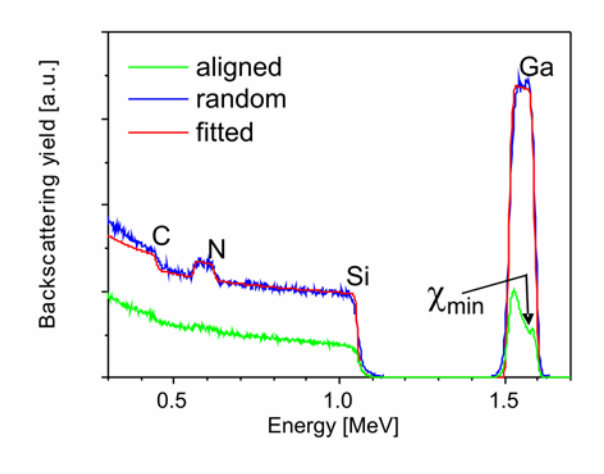

Fig. 6: Hexagonal $\{10\bar{1}1\}$ and cubic {111} pole figures of a 29 nm thick GaN film containing a mixture of both polytypes.

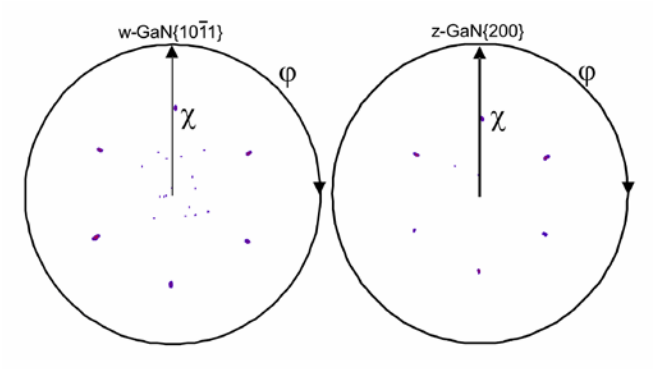

Fig. 7: (a) Cross-sectional transmission electron micrographs of a GaN (film of type D) on the basal plane of 6H-SiC with the w-GaN a-axis as zone axis. (b) High-resolution cross-sectional TEM micrograph of the layered GaN film. (c) and (d) show details of the z-GaN/w-GaN interface and of a region near the w-GaN film surface, respectively. (e) SAED pattern corresponding to the micrograph (b).

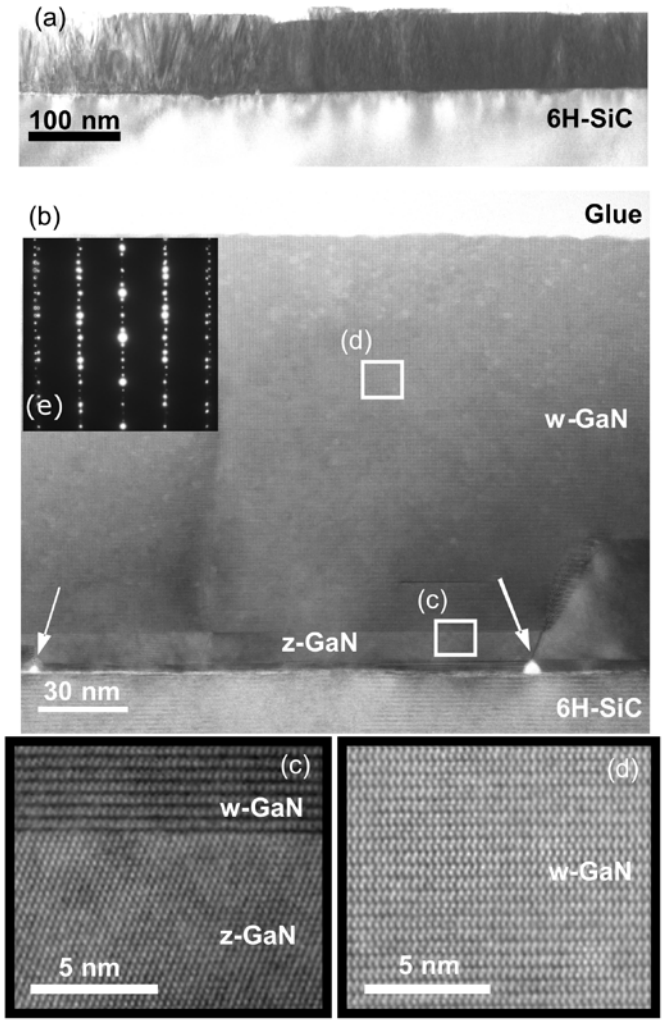

Fig. 8: Schematic of the transformation of Ga droplets into an epitaxial GaN film by low-energy nitrogen ion irradiation in the 2nd preparation step: (a) Initial state at the end of the 1st preparation step, (b) beginning nitrogen ion bombardment and nucleation of GaN crystallites at the peripheral region (the black arrows indicate the incoming nitrogen ion flux and the other arrows represent the most probable diffusion ways of adsorbed nitrogen species), (c) further growth of the GaN crystallites, (d) final state.

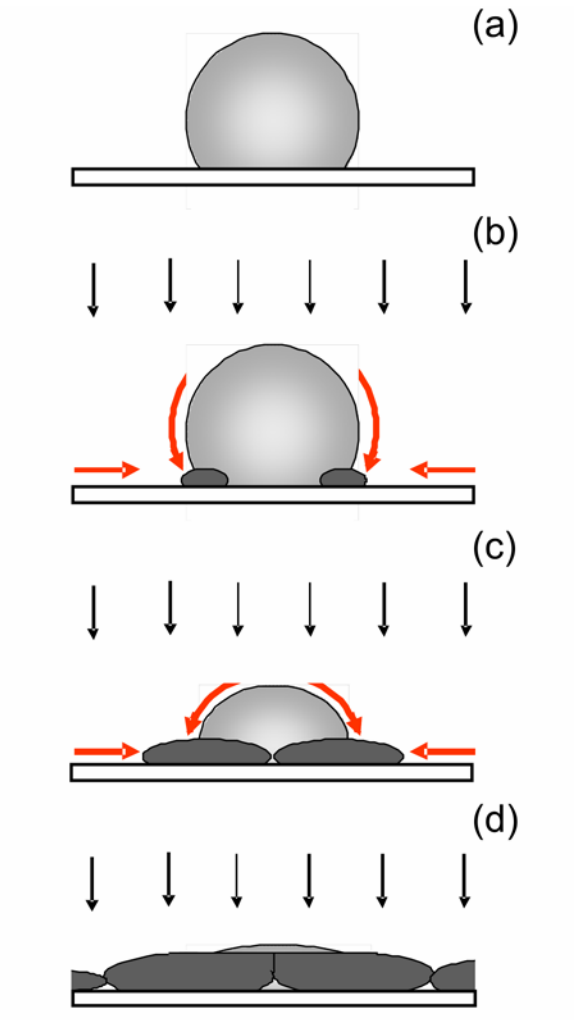

Fig. 9: Overview of the different diffusion fluxes involved in the nitridation process: flux J_{sp} of sputtered nitrogen atoms, flux J_d of nitrogen atoms diffusing into the Ga droplet, flux J_{cs} of nitrogen atoms diffusing on the Ga droplet surface, flux J_{ss} of nitrogen atoms diffusing on the substrate surface towards the Ga droplet. *R* is the droplet radius.